Trans. JSASS Aerospace Tech. Japan
Vol. 12, No. APISAT-2013, pp. a93-a98, 2014

Parametric Airfoil Representation toward Efficient Design Knowledge Discovery under Various Flow Condition*

By Masahiro KANAZAKI,[1)] Takaya SATO[1)] and Kisa MATSUSHIMA[2)]

[1)]*Graduate School of System Design, Tokyo Metropolitan University, Tokyo, Japan*
[2)]*Faculty of Engineering, University of Toyama, Toyama, Japan*

(Received February 6th, 2014)

The design of novel airfoils for airplanes invariably demands new knowledge of aerodynamics. PARametric SECtion (PARSEC) airfoil representation is one of the most promising methods for automated airfoil/wing design. However, because the airfoil parameterization was originally carried out for transonic flows, it may be difficult to extend its application to unknown flow conditions, including the low Reynolds number (*Re*) flow case. In this study, the representation of the PARSEC method is modified, especially around the leading-edge and applied to airfoil design using a multi-objective genetic algorithm, leading to an optimal design for potential development and use in a Martian airplane. Correspondingly, an airfoil that can obtain a sufficient lift and glide ratio under lower thrust conditions is considered. The objective functions aim towards maximizing the maximum lift-to-drag ratio generated and towards minimizing the drag at the maximum lift-to-drag ratio. In this way, information on the low *Re* airfoil could be extracted efficiently. The optimization results indicate that an airfoil with a sharper thickness at the leading-edge and a higher camber at the trailing-edge is more suitable for a Martian airplane.

Key Words: Airfoil Representation, Aerodynamic Design, Martian Airplane

1. Introduction

The advent of computational fluid dynamics (CFD) and its widespread use for airfoil design have facilitated more efficient airfoil representations, often required in airplane construction. A popular method for automated airfoil/wing design is PARSEC airfoil representation.[1)] However, its applicability to conditions other than the originally parameterized setting for transonic flow applications, such as the low Reynolds number (*Re*) flow case, should thus be further investigated. The performance of PARSEC airfoil representation is low around its leading-edge and it may thus be difficult to represent thin airfoil/wings that have a higher camber for low *Re* flows. To allow the design of a generic airfoil, modification of the PARSEC method has been proposed,[2)] yielding better design results for low *Re* flow cases.

Recently, many Mars exploration projects have been carried out around the world. For example, in Japan, the Institute of Space and Aeronautical Science (ISAS)/Japan Aerospace Exploration Agency (JAXA) proposed the Mars Exploration with Lander–Orbiter Synergy (MELOS)[3)] project. This project would use a Martian airplane to explore Mars, although many other exploration approaches (by the orbiter, by the lander, etc.) are considered. The Martian airplane gives the possibility to obtain high-quality and wide-scale geological information; however, its development requires the use of a brand new airfoil type, operating under unknown aerodynamic conditions.

In this study, a modified PARSEC method incorporating an additional parameter for the leading-edge is applied to airfoil design, using a multi-objective genetic algorithm (MOGA), with the aims of a) optimal airfoil design/performance at low *Re* flows and b) investigation of the proposed parameterization, for possible subsequent application on a Martian airplane. At first, optimization using a fully turbulent solver is carried out with a low-cost approach, and the aerodynamic performances of the optimal designs are investigated by a laminar flow solver. The elicited performances of studied airfoils using the proposed representation are compared with the high-performance Ishii airfoils[4)] used for a hand-launch glider.

2. Airfoil Representation Methods

2.1. Original PARSEC method

The original PARSEC method[5)] mathematically represents a supercritical airfoil based on a polynomial function. This method defines the upper and lower airfoil surfaces and connects the leading-edge successively (Fig. 1). The airfoil representation function at the x–z plane can be written as

$$z = \sum_{n=1}^{6} a_n x^{\frac{2n-1}{2}} \tag{1}$$

The a_n values are determined from 11 structural parameters, as shown in Fig. 1.

*Presented at the 2013 Asia-Pacific International Symposium on Aerospace Technology (APISAT-2013), Nov 20-22, 2013, Takamatsu, Japan

2.2. Modified PARSEC method

Although the center of the leading-edge radius, r_{le}, has been originally defined on a camber line, the original PARSEC method postulates that r_{le} is on the chord line. Therefore, the representation performance of an airfoil, based on the original PARSEC method with a high camber around the leading-edge, is low. To improve performance around the leading-edge, the airfoil's thickness and camber should be separately defined, as shown in Figs. 2 and 3. The thickness distribution is defined by Eq. (2), corresponding to a symmetrical airfoil using the original PARSEC method, represented in accordance qith Eq. (1).

$$z = 2\sqrt{2r_{le}x} + \sum_{n=1}^{5} a_n x^{\frac{2n-1}{2}} \tag{2}$$

The camber distribution is defined using Eq. (3).

$$z = \mathrm{sgn}(r_c)\sqrt{2|r_c|x} + \sum_{n=1}^{5} b_n x^n \tag{3}$$

The a_n and b_n values of Eqs. (2) and (3) are determined from 12 structural parameters, as shown in Figs. 2 and 3.

It is important to control the LE camber (which can control the LE suction) as well as the TE camber (which can maintain Kutta's condition) in view of drag reduction (or *l*/*d* improvement). A square root term is added to the camber's representation (see Eq. (3)) to improve representation performance around the leading-edge using the radius of the camber at the leading-edge, and r_c. "sgn" in Eq. (3) is the sign function (signum function). The large coefficient of the first term of Eq. (3) gives weight to the design of the LE camber as shown in Fig. 4(a). If the first term of Eq. (3) is negative, the airfoil has a negative camber around the leading-edge, as shown in Fig. 4(b).

In this study, the modified PARSEC method whose r_c does not become negative is called "Case 1," while the modified PARSEC method whose camber r_c become negative is called "Case 2." The design results obtained by "Case 1" and "Case2" are compared and the effect of representing the camber around the leading-edge is investigated.

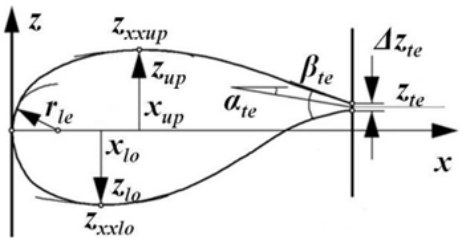

Fig. 1. Original PARSEC method.

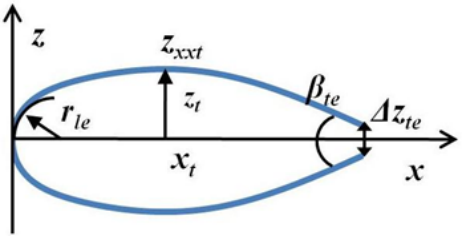

Fig. 2. Modified PARSEC method (thickness distribution).

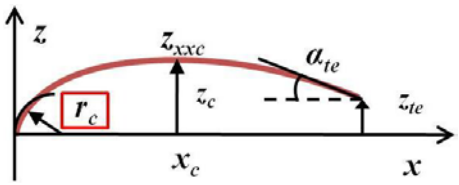

Fig. 3. Modified PARSEC method (camber distribution).

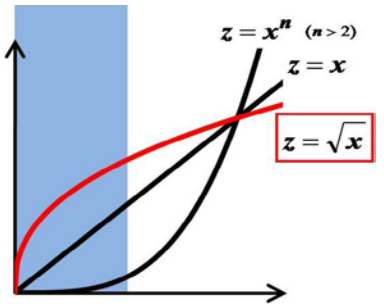

(a)

(b)

Fig. 4. Modification of representation around the leading-edge. (a)Control of the leading-edge radius using $\sqrt{x}$ and (b)Design of negative camber around the leading-edge.

3. Analysis Method

3.1. Aerodynamic evaluation

The aerodynamic evaluation was carried out using a two-dimensional Reynolds-averaged Navier–Stokes solver (RANS), for which the governing equation is expressed as

$$\frac{\partial}{\partial t}\int_{\Omega} \Phi dV + \oint_{\partial\Omega} F \cdot n ds = 0 \tag{4}$$

Φ is a vector that consists of a conservative quantity, and F is the summation of the conservative quantity traversing (passing through) the area. A Lower–Upper Symmetric Gauss–Seidel (LU-SGS) implicit method is employed for time integration, and an accurate third-order upwind differential scheme[6] with a Monotone Upstream-centered Scheme for Conservation Laws (MUSCL) method is employed for the flux evaluation. The Baldwin–Lomax model is used as a turbulent model. Because the convergence of the fully turbulent solver is faster than that of the laminar flow solver, the turbulent flow solver is employed in the Multi-Objective Genetic Algorithm (MOGA) process. After the optimal solutions are obtained, their performances are also investigated using the laminar solver, because this study also considers low *Re* flow conditions.

For all analyses, a structured grid is employed for space discretization. The grids are automatically created by an

algebraic method; the structured grid for the RANS is 128 × 61 (see Fig. 5).

3.2. MOGA

In this study, the optimization is completed using NSGA-II.[7] MOGA is an algorithm inspired by the evolution of a living organism's adaptation to the environment. It possesses a high ability to solve multi-objective problems that are nonlinear and is capable of searching for global solutions. A flowchart of the MOGA execution is shown in Fig. 6. The number of populations for the first generation is 10, and the number of generations is 100.

3.3. Parallel coordinate plot (PCP)

A PCP[8] is a statistical visualization technique used for reducing high-dimensional data into two-dimensional data. Based on this method, the design variables and objective functions are set parallel to the normalized axis within each design space. Therefore, a PCP shows the global trends of design variables and objective functions, as shown in Fig. 7.

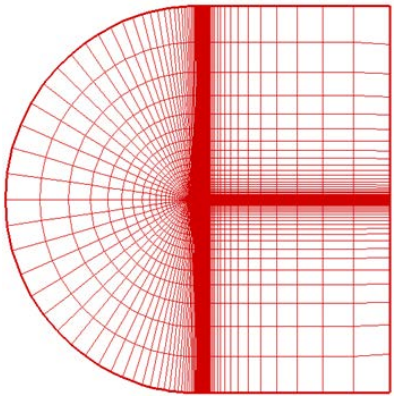

Fig. 5. Grid resolutions for MOGA evaluation.

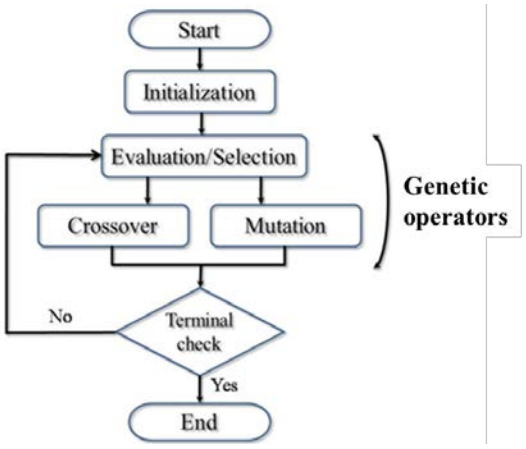

Fig. 6. Flowchart of MOGA.

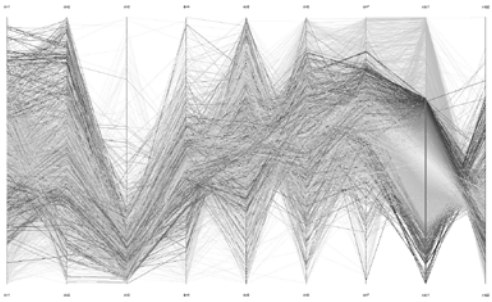

Fig. 7. Visualization example using the PCP methodology.

4. Formulations

The proposed methodologies adopted in this study are demonstrated by designing a low *Re* and a low speed-of sound-airfoil, and by considering its implementation on a Martian airplane, through comparisons with the two proposed design methods, namely, cases 1 and 2. To allow the implementation of an airfoil that achieves a high glide ratio and low drag, under the unknown conditions of the Martian atmosphere, two objective functions are considered: a) maximizing of the lift-to-drag ratio (*maxl*/*d*), and minimizing of the drag at *maxl*/*d* (C_d@*maxl*/*d*) conditions as in Eq. (6).

$$\begin{cases} \text{Maximize } max/d \\ \text{Minimize } C_d@maxl/d \end{cases} \tag{6}$$

Because Δz_{te} is fixed at 0.01 and the airfoil thickness is fixed at 7% *c*, only the remaining 10 parameters are set in the proposed representation. The computational conditions include a Mach number M = 0.2 and a *Re* of 2.3 × 10^4. Table 1 shows the design space for cases 1 and 2.

Table 1. Design space (modified PARSEC 1 and 2).

Design variables			Lower	Upper
Thickness	Radius at LE	r_{le}	0.0001	0.006
	x-coord. of max. thickness	x_{up}	0.200	0.600
	Curvature at max. thickness	z_{xxup}	-0.900	-0.400
	Angle of TE	β_{te}	0.5000	10.000
Camber	Camber radius at TE	r_c	0.000 (mod 1) -0.004 (mod 2)	0.004
	x-coord. of max. camber	x_c	0.300	0.400
	z-coord. of max. camber	z_c	-0.030	0.030
	Curvature at max. comber	z_{xxc}	-0.250	0.010
	z-coord. of TE	z_{te}	-0.040	0.010
	Angle of camber at TE	α_{te}	4.000	15.000

5. Results

5.1. The optimizations by MOGA

Figure 8 shows the optimization results. In Fig. 8 (a), red dots are the non-dominated solutions of Case 2, yellow dots are the non-dominated solutions from Case 1, and the green dot represents the performance of the Ishii airfoil. Numerous solutions dominate the Ishii airfoil design, from both Case 1 and Case 2 representations. In addition, the solutions in Case 2 outperform those in Case 1 solutions. Such findings suggest that the proposed method has an advantage in designing better airfoils operating in low *Re* flows.

Des1, Des2, and Des3 are selected as the airfoil designs resulting from the non-dominated solutions in Case 2, as shown in Fig. 8(b). Two additional designs are also chosen from the non-dominated solutions obtained in Case 1. Figure 9 shows a comparison of the airfoils obtained from cases 1 and 2. Specifically, Fig. 9(a) shows the performance comparison of the airfoils designed in Case 1 and Case 2 (Des1) in respect to the highest *maxl*/*d* value. Figure 9(b) shows the comparison results of the lowest attained C_d value,

between the chosen airfoil designed using the modified PARSEC 1 and PARSEC 2 (Des1) methods. According to Fig. 9(a), the thickness around the trailing-edge of Des1 becomes thinner than that of the modified PARSEC 1. Namely, the proposed representation has the advantage of local control of the geometry through the extension of the camber representation. According to Fig. 9(b), the thickness around the trailing-edge of Des1 also becomes thinner than that of the modified PARSEC 1. In addition, the maximum camber is lower than that of Case 1, while two airfoils achieve similar *maxl*/*d* values. This result suggests that Case 2 could represent a more efficient airfoil that can simultaneously achieve a higher lift and lower drag with a lower maximum camber.

Table 2 shows the comparison of aerodynamic performances. The generated *maxl*/*d* value of Des1 is about twice as that of the Ishii airfoil, and the C_d@*maxl*/*d* of Des3 is about one-half that of the Ishii airfoil.

5.2. Visualization of non-dominated solutions using a PCP

The trend for each design variable and the objective functions of the solutions are visualized using a PCP, as shown in Fig. 10. Figure 10(a) shows the PCP visualization of all solutions obtained using the MOGA, and Fig. 10(b) shows the PCP visualization of Pareto solutions. Figures 10(a) and 10(b) are plotted in terms of *maxl*/*d*, which is one of the objective functions. As Fig. 10(a) shows, the solutions obtained were widely distributed in the design space and gradually converged toward the optimum *maxl*/*d*. For example, the design that yields the wrong *maxl*/*d* has the lowest value of the maximum camber z_c (approximately -0.22). The solutions that yield better *maxl*/*d* values have relatively high z_c values (approximately 0.008 to 0.28). These results suggest that the proposed airfoil representation offers the advantage of maintaining a high diversity and is suitable for use in design problems below an unknown point.

As Fig. 10(b) shows, the radius at the leading-edge r_{le} becomes approximately zero. This suggests that an airfoil with a sharper thickness at the leading-edge is better for a Martian airplane. In addition, the angle of the trailing-edge β_{te} and the *z*-coordinate of the trailing-edge z_{te} become relatively low, and the angle of camber at the trailing-edge α_{te} becomes high. This suggests that a thinner airfoil with a higher camber around the trailing-edge is better for a Martian airplane.

The results obtained suggest that the proposed modified method affords a high degree of freedom in airfoil representation, especially around the leading-edge and trailing-edge.

5.3. Comparison of geometry and aerodynamic performance

The airfoil geometry and pressure distribution, C_p, of the selected designs are also compared. C_p is evaluated in a laminar flow setting, without the use of turbulent models, using a 498 × 99 grid (Fig. 11).

Figure 12 shows the airfoil geometries and C_p distributions of designs Des1, Des2, Des3 and the Ishii airfoil. Table 3 shows comparisons of the aerodynamic performances. Comparing Tables 2 and 3, the rank of the aerodynamic performances using the laminar flow evaluation scheme is the same as that using the turbulent slow solver. As shown in Fig. 12, the airfoils designed by the proposed method have a sharper thickness at the leading-edge and a higher camber curve at the trailing-edge. This agrees with the design space visualization shown in Fig. 10. In addition, the resulting C_p distribution suggests that Des1 and Des2 obtain higher lift around the trailing-edge compared to the Ishii airfoil. On the other hand, Des3, which achieves the lowest C_d@*maxl*/*d*, shows a low suction peak compared to the Ishii airfoil. Because of this lower suction peak, Des3 can achieve a lower drag.

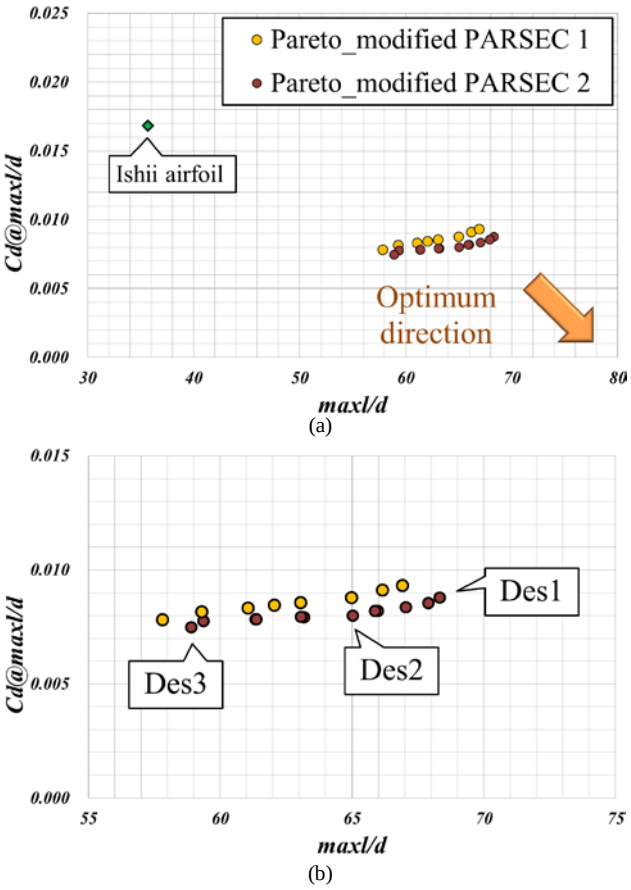

Fig. 8. Optimization results using MOGA. (a) Non-dominated solutions for Case 1 and Case 2. The green dot represents the Ishii airfoil condition (baseline). (b) Close-up view around non-dominated solutions.

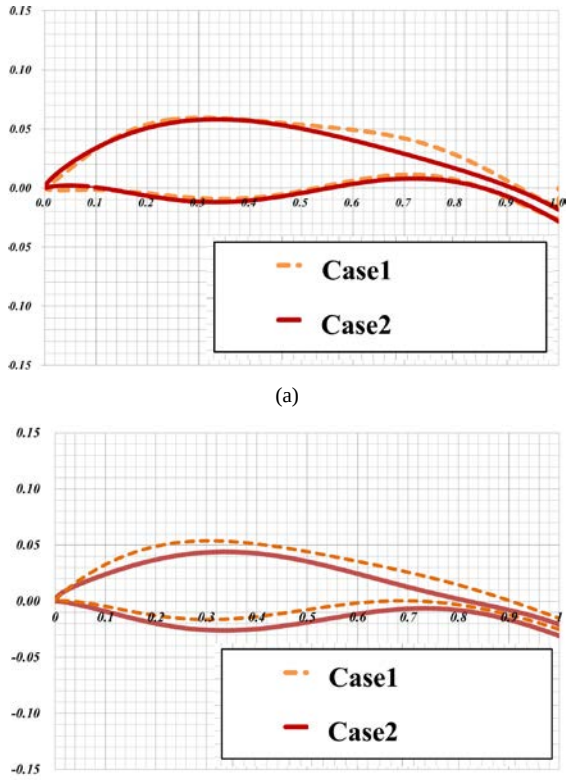

(a)

(b)

Fig. 9. Comparison of airfoils obtained by the two adopted representation methods (Case 1 and Case 2). (a) Design results which achieve the highest *maxl*/*d* value, and corresponding (b) design results which achieve the lowest C_d.

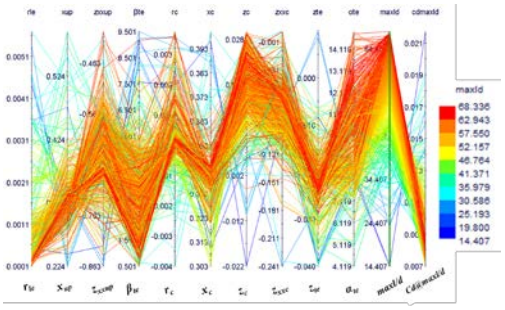

(a)

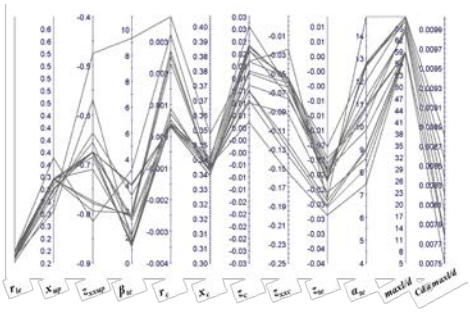

(b)

Fig. 10. Visualization by PCP for Pareto solutions. (a)All non-dominated solutions colored by *maxl/d* and (b)Non-dominated solutions which is sorted by *maxl/d*.

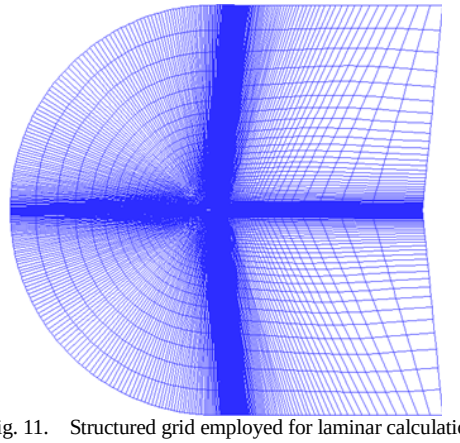

Fig. 11. Structured grid employed for laminar calculation.

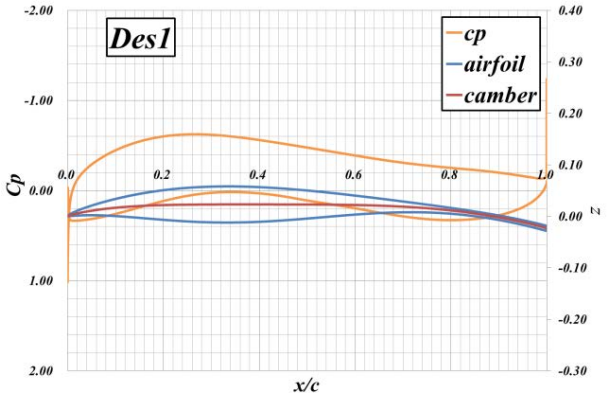

(a) Des1

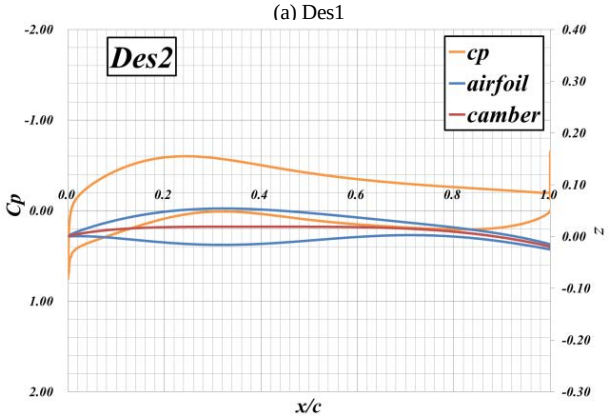

(b) Des2

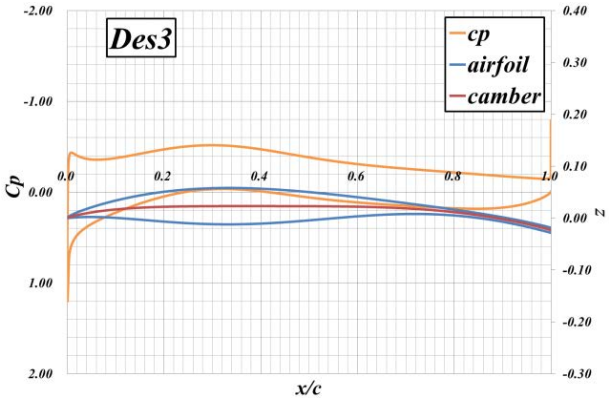

(c) Des3

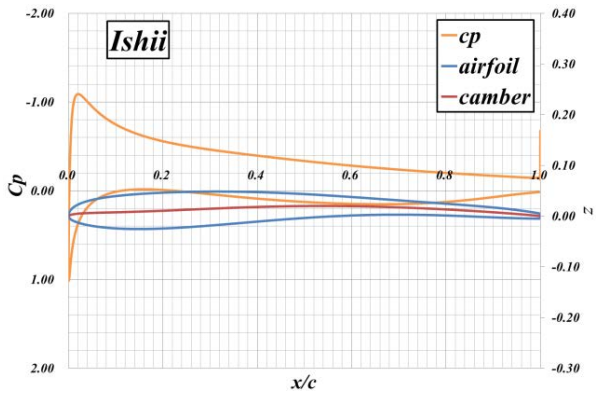

(d) Ishii airfoil

Fig. 12. Airfoil configuration and C_p distribution of representative airfoil designs (Des1, Des2, Des3) at *maxl*/*d* (laminar flows).

Table 2. Aerodynamic performance of representative airfoil designs obtained by MOGA using the RANS. (AoA is the angle of attack when the airfoil achieves maximum *l*/*d*.)

	maxl/*d*	C_d@*maxl*/*d*	AoA [deg]
Des1	68.33	0.0088	2.24
Des2	65.04	0.0080	1.99
Des3	58.91	0.0074	2.31
Ishii	35.69	0.0168	4.18

Table 3. Aerodynamic performance of representative airfoils evaluated under laminar flow conditions.

	maxl/*d*	C_d@*maxl*/*d*	AoA [deg]
Des1	27.94	0.0157	3.14
Des2	27.64	0.0156	2.97
Des3	25.17	0.0149	3.41
Ishii	18.36	0.0239	3.10

6. Conclusion

In this study, a modified PARSEC method is developed to facilitate the design of the optimum airfoil for use under unknown flow conditions, including a low *Re* flow case. This study considers a high-performance airfoil under low *Re* flow conditions that can be potentially used for a Martian airplane. The MOGA is used for the optimization, and the generated results are compared to the optimization obtained using modified PARSEC 1 and 2 methodologies. The design objectives are maximizing the maximum *l*/*d* and minimizing C_d at the maximum *l*/*d*.

The design results suggest that the modified PARSEC 2 can lead to an airfoil with improved performance under low *Re* conditions compared to PARSEC 1, primarily due to the increased degree of freedom for airfoil representation, yielding improvements around the leading and trailing-edges. Also suggested is that the modified PARSEC 2 can determine the ideal airfoil design under unknown flow conditions.

Investigating the designed airfoils and their flow fields showed that an airfoil with a sharper thickness at the leading-edge and a higher camber at the trailing-edge achieves higher *maxl*/*d* values, rendering it as an airfoil giving a better performance under low *Re* conditions, and illustrating the suitability for possible use in a Martian airplane.

References

1) Sobieczky, H.: Parametric Airfoils and Wings, *Notes on Numerical Fluid Mechanics*, Springer, Vol. 68 (1998), pp. 71-88.
2) Tomoyoshi, Y., Kanazaki, M. and Matsushima , K.: Design Performance Investigation of Modified PARSEC Airfoil Representation Using Genetic Algorithm, Eurogen 2011 Conference, Capua, Italy, 2011.
3) Ogawa, J., Kubota, T., Hujita, K., Yamada, T., Katsukawa, Y., Ishii, N., Kawaguchi, J. and Sato., K.: Outline of Mars Exploration with Lander-Orbiter Synergy (MELOS), JSASS-2009-4093, 2009.
4) Nonomura, T., Kojima, R., Anyoji, M., Oyama. A. and Fujii. K.: Aerodynamic Characteristics of Ishii Airfoil (Re=23,000) using LES, The 43th Aero Numerical Simulation Symposium 2011, JAXA-SP-11-015, 2012, pp. 43-48.
5) Matsushima, K., Matsuzawa, T. and Nakahashi, K.: Application of PARSEC Geometry Representation to High-Fidelity Aircraft Design by CFD, The 8th WCCM8/ 5th ECCOMAS, 2008.
6) Obayashi, S. and Guruswamy, G. P.: Convergence Acceleration of an Aeroelastic Navier-Stokes Solver, *AIAA J.*, **33** (1995), pp. 1134-1141.
7) Deb, K., Agrawal, S., Pratap, A. and Meyarivan, T.: A Fast Elitist Non-Dominated Sorting Genetic Algorithm for Multi-Objective Optimization: NSGA-II, KanGAL Report No. 200001, (2000), Indian Institute of Technology, Kanpur, India.
8) Wegman, E. J.: Hyper-dimensional data analysis using parallel coordinates, *Journal of American Statistical Association*, Vol. 85, No.411, (1990), pp.664-675.